

# Numerical evaluation of the exact phase diagram of an empirical Hamiltonian: Embedded atom model for the Au-Ni system

E. Ogando Arregui,<sup>1</sup> M. Caro,<sup>2,3</sup> and A. Caro<sup>2,3</sup><sup>1</sup>*Dep. de Electricidad y Electrónica, UPV-EHU apdo. 644, 48080 Bilbao, Spain*<sup>2</sup>*Centro Atómico Bariloche, 8400 Bariloche, Argentina*<sup>3</sup>*Atomistic Simulation Group, The Queen's University, Belfast, Northern Ireland, United Kingdom*

(Received 1 November 2001; revised manuscript received 19 February 2002; published 2 August 2002)

Molecular-dynamics simulations were used to calculate the Gibbs free energy on the entire compositional range of gold-nickel alloys described with a set of embedded atom potentials available in the literature. Thermodynamic integration and switching Hamiltonian techniques were used to obtain the exact phase diagram (with no approximations), and that corresponding to the regular approximation. Remarkable agreement for some properties, such as the *solvus* critical point, the congruent melting, the melting points of the pure elements, and the formation entropy of the alloy, contrasts with the poor prediction of the location of the *solidus-liquidus* lines, reflecting errors in the heat of solution in the liquid phase. The results are compared with recent experimental reassessment of the Au-Ni phase diagram and with *ab initio* calculations.

DOI: 10.1103/PhysRevB.66.054201

PACS number(s): 81.30.Bx, 82.60.Lf, 02.70.Ns, 64.75.+g

## INTRODUCTION

The classic many-body potentials, known generically as the embedded atom model (EAM), provide a powerful tool to study several types of simple solids, in particular, transition metals and some of their alloys.<sup>1-3</sup> Extensive work has been done in the application of this model to many solid solutions and intermetallic compounds, but limited effort was devoted to the computational calculation of the complete equilibrium phase diagram predicted by this type of approximation. Therefore, little is still known about the ability of the  $n$ -body potentials to reproduce details of the equilibrium phase diagrams of transition metal alloys.

In recent times, several articles appeared showing procedures to evaluate numerically the free energy, using both *ab initio* and empirical descriptions for the total energy, either in molecular-dynamics (MD) or Monte Carlo frames (MC). The use of these techniques has been proposed to increase the precision of the empirical Hamiltonians by incorporating, for example, the thermodynamic melting temperature in the fitting procedure.<sup>4</sup> Specific intermetallics, in particular in the Al-Ni system, have received a lot of attention and consequently sets of potentials specially suited for some phases are available in the literature.<sup>5</sup> However the reciprocal problem, i.e., what kind of phases are predicted by a given set of potentials, is much less known. The interest in the answer to this question is not only natural curiosity, but has outmost relevance in applications where the results depend on thermodynamic driving forces derived from the equilibrium phase diagram. One such case is the application of EAM potentials to radiation damage problems, where the solid target is driven far from equilibrium by an energetic projectile.<sup>6</sup> Another example is the structure of nanophase metallic alloys, where interface segregation and the nature of the phase diagram at such small scales is an issue on discussion.<sup>7,8</sup>

The Au-Ni system has a simple phase diagram but unusual thermodynamic properties in the sense that it exhibits a large positive enthalpy of mixing originated in the significant size mismatch effect, and large positive excess entropy reflecting a change in the vibrational frequency spectrum on

alloying. This system has received a lot of attention from three different avenues: experimental, *ab initio*, and empirical potential calculations. Unfortunately, the present state of the art of the *ab initio* calculations for alloys is still insufficient to accurately reproduce all the features of the phase diagram, formation enthalpies, entropies, miscibility gap, and tendency to order. For a review of the performed work, see Refs. 9, 10.

The main features of the diagram are a wide miscibility gap, and a broad and deep minimum in the liquidus line. Controversies about the location of the solidus as well as on the eventual order in the solid solution have lead to several studies starting in 1955.<sup>11-14</sup> The standard phase diagram for this system is that of Okamoto and Massalski.<sup>15</sup> Recently, Bienzle *et al.*<sup>16</sup> published a reassessment of the entire diagram combining electromotive force, differential thermal analysis, x-ray diffraction, and transmission electron microscopy measurements to determine the phase boundaries in the solid and liquid, and the microstructure of the Au-rich solid solutions. They also provide values for the excess enthalpy and entropy of mixing that, being positive, cause the large miscibility gap. The excess enthalpy of the liquid phase is also positive although smaller than the solid value, and accounts for the minimum at the congruent point. Some short-range order (SRO) above the miscibility gap is also reported, ruling out claims on clustering of like atoms,<sup>17-21</sup> or even the presence of intermetallic phases.<sup>22</sup> The diversity of experimental observations is accompanied by a significant uncertainty in the theoretical evaluations that comes from the fact that in this system the formation enthalpy is the result of the cancellation of two large terms: a large and positive value coming from the elastic lattice distortion due to different atomic radii (Au 1.46 Å and Ni 1.24 Å) and a negative chemical contribution (estimation based on electronic calculations in Ref. 23), in accordance with the difference in the electronegativity of the pure elements. According to Lu and Zunger,<sup>24</sup> systems with different sign in these two contributions may show phase separation in the long-range order (LRO) at low  $T$ , and ordering in the SRO at high  $T$ , while phase separation/clustering is shown for systems where both

contributions have equal sign (either positive or negative). Therefore, the competition between the accuracy used in the different stages of the modeling ends up with controversial conclusions. Ordering appears clearly in Au-Ni thin films, as recent experimental behavior reports, which is explained in terms of epitaxial strain stabilization.<sup>25</sup>

First-principles theoretical determinations of the phase diagram mainly address the issue of order in the solid phase. In 1994 Amador and Bossolo<sup>26</sup> use linear muffin-tin orbital (LMTO), together with the cluster expansion for the energy calculations and the cluster variational method for the free energy calculations, to determine the formation energy of the random alloy, concluding that the SRO is almost null due to the low (positive) formation energy; their values for the formation energy, however, are a factor of 3 greater than the experimental ones due to the large mismatch present in this system and the lack of relaxation in their method. Also Colinet *et al.*<sup>27</sup> published a calculation based on the same *ab initio* method [LMTO atomic-sphere approximation (ASA)] and cluster techniques, incorporating lattice relaxation and vibrational effects through a Debye-Grüneisen model. Their prediction for the formation energy of the random solution is in excellent agreement with the experimental values. Additionally, the miscibility gap derived from it, when vibrational entropy is included, also agrees very well. Interesting to mention is the fact that the formation energy reported in that work is almost symmetric in the concentration axis, as is the configurational entropy; the asymmetry in the solvus curve mainly comes from the positive vibrational entropy contribution. However, some years later<sup>28</sup> the same group published a better calculation based on LMTO full potential (FP) and the results depart from the experiments in the same sense than in the Ref. 26, i.e., the formation energies are smaller than the measured values. The new miscibility gap shows a critical temperature 150 K above the experimental value, and for this calculation the formation energy and vibrational entropy are both responsible for the asymmetry in the miscibility gap. Finally, they also arrive at the conclusion that the ordering tendency has a rather negligible contribution and can be neglected in the free energy calculations.

Wolverton *et al.*<sup>29</sup> describe a first-principles technique to calculate SRO for several systems, in particular Au-Ni. They build an Ising Hamiltonian based on a FP-LAPW and a mixed space cluster expansion, that incorporates the relaxation in the parameter evaluation step, and which is used in lattice MC runs in the canonical ensemble with sample sizes between 15–30 thousand atoms. They compare their value of the Warren-Cowley SRO for the first shell (110),  $-0.024$  (slight ordering tendency), with the experimental results of Wu and Cohen from 1983 (Ref. 30) at  $T=1023$  K and composition  $X_{\text{Ni}}=0.4$  which is  $0.039$  (slight clustering tendency). The agreement on the second shell is much better and of more significance (calculated  $0.12$ , experimental  $0.15$ ) showing a clustering type ordering. It is a surprising characteristic of this alloy that being phase separating, shows some shells with tendency to order.

The use of computer simulations to calculate thermodynamic properties of solids has a long history either via MC as well as MD. In the beginning of the 1980's, hard spheres and

other simple models of solids were explored and powerful algorithms were deduced. Among them, Frenkel and Ladd introduced a method to calculate absolute free energies of arbitrary solids based on the construction of a reversible path from the solid phase under consideration to an Einstein crystal with the same crystalline structure.<sup>31</sup> Their reversible path method, with some modifications, is one of the most common methods used today, either in MC and MD. With equivalent methods for the liquid phase, the equilibrium phase diagram of a given model Hamiltonian can be constructed. We note that for this purpose, absolute values of the free energies in the coexisting phases have to be known. Kranendonk and Frenkel<sup>32</sup> reported the first calculation of the solid-liquid coexistence in binary hard spheres mixtures with these methods. Mei and Davenport<sup>33</sup> calculated the melting point of Al predicted by an EAM potential using MD and the ideal gas as a reference system for the liquid phase. Recently, Sturgeon and Laird used this method to modify the Mei and Davenport potential for Al to better reproduce its melting point.<sup>4</sup> As an alternative to MD, Lynden-Bell *et al.*<sup>34</sup> used a biased potential in a MC simulation with umbrella sampling to determine the Landau free energy in terms of order parameters that describe the crystalline and the liquid order in terms of the symmetry of the bonds. With it, the thermodynamic melting and the limit of metastability of the crystalline phase of several ductile metals described by EAM-type potentials were determined. de Koning and Antonelli<sup>35</sup> analyze the behavior of Einstein oscillators as a reference system in adiabatic switching, using the canonical massive Nosé-Hoover chain dynamics. They arrive at an estimation of the error in the procedure, allowing a correction of the converged results. With this formalism, they study the vacancy free-energy formation in copper.<sup>35,36</sup> de Koning *et al.* proposed an optimized free energy evaluation based on the switching Hamiltonians, but in such a way that the switch and the temperature variation are both tackled in a single MD run, improving significantly the efficiency of the method.<sup>37</sup> They apply the method to evaluate the free energy of crystalline Si with empirical potentials. A MC improvement that also involves a single simulation was proposed and applied by Bruce *et al.* to the free energy difference between the fcc and hcp structures of hard spheres.<sup>38</sup>

Another widely used approach to free energy calculations is the quasiharmonic approximation. In this method, a free energy is evaluated separately as the contribution from the enthalpy (directly accessible from the simulation) and the vibrational entropy, through lattice dynamics in the quasiharmonic approximation. Examples of application are the temperature dependence of the elastic constants of Au, the surface energy of Cu, the thermal expansion of  $\text{Cu}_3\text{Au}$  by Barrera and Tendler,<sup>39</sup> the structure and energetics of Cu-Au alloys by Barrera *et al.*<sup>40</sup> (which reproduce correctly the nature of the order-disorder transition), and the phase diagram on the MnO-MgO system, that contains a miscibility gap.<sup>41,42</sup>

With a mixed *ab initio*-classical potential and lattice dynamics-MD, a fully theoretical prediction of thermodynamic properties of Al, including a melting point within 2.5% of the experimental value, was presented by Straub

*et al.* in 1994.<sup>43</sup> De Wijs *et al.* also made *ab initio* calculations of the same metal using coupling constant integration with the quasiharmonic crystal and the Lennard-Jones fluid as reference states, again proving the power of the method to predict basic thermodynamic properties.<sup>44</sup>

From the phenomenological avenue, the embedded-atom-type description of the Au-Ni system starts with the paper by Foiles *et al.*<sup>45</sup> describing a set of potentials for the transition metals of the Ni and Cu columns, and their dilute alloys. In this set, they adjusted the potentials to several properties of the pure elements as well as the heat of solution of their alloys. Later, Foiles and Adams evaluated thermodynamic properties of the same elements using these potentials.<sup>46</sup> They use a quasiharmonic approximation for the free energy of the solid phases and grand canonical Monte Carlo for the liquid phase; they also use MC to get the free energy of the solid and find good agreement between the two techniques. For the particular case of Ni, the free energies they get are greater than the experimental values in both solid and liquid phases, and this error is the largest for all the elements considered. Fortuitously, the reported melting point for pure Ni, 1740 K, is in very good agreement with the experiment because the errors in the liquid and solid free energies cancel one another. For Au, both free energies are less than the experimental values, as is the melting point 1090 K (18% below). Recently, Asta and Foiles<sup>47</sup> studied three phase separating solid solutions, including Au-Ni. They developed a second-order energy expansion to treat compositional and displacive disorder casting the problem in the form of a lattice gas Hamiltonian with effective pair interactions. They developed a new potential for Au-Ni because the original one poorly described (underestimates) the excess heat of mixing of concentrated solutions. They obtained good agreement close to equiatomic solutions and a poor description for dilute ones. However, they were unable to calculate the solvus line because the alloy is unstable below the critical temperature  $T_c$ , which by the way, is 2 to 3 times larger than the experimental value.

In this work, we study one of the earliest embedded-atom (EAM) potentials developed by Foiles *et al.*<sup>45</sup> for Au-Ni to extract its phase diagram. In this way, this work contributes to the knowledge of the EAM approach to describe metallic alloys.

We report Gibbs free energies calculated using MD simulations for pure elements and for several Au-Ni alloys. We follow the procedure described by Mei and Davenport<sup>33</sup> and apply it to alloys with different nickel concentration. To our knowledge these are the first calculations of the exact free energy of the alloy and with it, the exact phase diagram of a model Hamiltonian. By exact we mean no approximations in the formalism, such as the well-known quasiharmonic approximation. The numerical evaluations, on the contrary, have dispersion originated in either the finite size of the samples, and the finite time used in the averages.

### FREE-ENERGY CALCULATION—PURE ELEMENTS

Calculating free energies involves the computation of the partition function by integrating over the entire phase space

of a system with a large number of degrees of freedom. Since this is impossible to do computationally for *ab initio* Hamiltonians, approximate schemes such as those mentioned above are used. For empirical Hamiltonians, however, an almost direct calculation of the free energy is possible and is the approach taken in this work.

In the derivations that follow, as well as in the comparison with experiments, we shall not make a distinction between Gibbs and Helmholtz free energies, as well as internal energy and enthalpy, because some integrals or averages can be better calculated at constant  $V$ , and others at constant  $P$ . The difference between these magnitudes is equal to  $PV$ , which is negligible compared to value and error of the variables, except at very high pressures. For clarity, however, steps are formulated in terms of  $f$  or  $g$  to make it explicit the ensemble where the calculation is done.

Let us concentrate first on pure elements to introduce the general procedure, and then we will focus on alloys. We calculate the free energy per particle at a given temperature  $T$ ,  $f(T)$ , through thermodynamic integration between the state of interest and a reference state at temperature  $T_0$  with known free energy  $f(T_0)$ . The free energy per particle is given by the Gibbs-Duhem integral

$$f(T) = f(T_0) \frac{T}{T_0} - T \int_{T_0}^T \frac{h(\tau)}{\tau^2} d\tau, \quad (1)$$

where  $h(\tau)$  is the enthalpy per particle.

The coupling-constant integration method, or switching Hamiltonian method,<sup>48</sup> is used to calculate  $f(T_0)$ . We consider a system with Hamiltonian  $H = (1 - \lambda)W + \lambda U$ , where  $U$  describes the actual system (in this work, EAM Hamiltonian) and  $W$  is the Hamiltonian of the reference system, with known free energy. With this Hamiltonian we can calculate the free energy difference between  $W$  and  $U$  calculating the reversible work required when switching from one to the other. This switch has to be reversible, free of any phase transition. Then the unknown free energy associated to  $U$ ,  $f(T_0)$ , is simply given by

$$f(T_0) = f_W(T_0) + \Delta f_1,$$

$$\Delta f_1 = \frac{1}{N} \int_0^1 \left\langle \frac{\partial H}{\partial \lambda} \right\rangle d\lambda = \frac{1}{N} \int_0^1 \langle U - W \rangle_\lambda d\lambda, \quad (2)$$

where  $f_W(T_0)$  is the free energy of the reference system at  $T_0$  temperature. The integration is carried over the coupling parameter  $\lambda$  varying between 0 and 1, and  $\langle \dots \rangle$  is the average over a canonical ensemble, or a time average on a  $(T, V, N)$  MD simulation.

For the solid phase it is customary to take as reference system a set of Einstein oscillators centered on the average positions of the atoms in the  $(T_0, P=0, N)$  ensemble corresponding to Hamiltonian  $U$ . The noninteracting Einstein oscillators have no internal pressure so the only possible ensemble is the  $(T, V, N)$ . The free energy of the Einstein crystal can be calculated analytically,<sup>49</sup>

$$f_W^{\text{sol}}(T_0) = f_{\text{Eins}}(T_0) = -3k_B T_0 \ln(T_0/T_E). \quad (3)$$

Here  $T_E$  is the Einstein temperature of the oscillators,  $T_E = \hbar\omega/k_B$ , where  $k_B$  is the Boltzmann constant,  $\omega$  is the frequency of oscillations, and  $\hbar$  is the Planck constant divided by  $2\pi$ .

For the liquid, the usual reference system  $W$  is an ideal gas at the same temperature and volume of the EAM sample. The process to switch from  $U$  to  $W$  involves an intermediate step to avoid particle overlap during the integration. First, we compute the free-energy difference between the true system with potential  $U$  (the EAM potential) and a system with a repulsive potential  $W_L$  (soft spheres). In this work, we use  $W_L = 0.1 U^{\text{rep}}$ , where  $U^{\text{rep}}$  is the pair potential part of the EAM energy, which is purely repulsive for the potential we are using.<sup>45</sup> The repulsive potential cannot be very strong because the sample may crystallize, an irreversible process. As in the solid phase, the integration is carried over the coupling parameter  $\lambda$  varying between 0 and 1. The system is kept at the constant volume  $V_0$ , that equilibrated the  $U$  Hamiltonian at temperature  $T_0$  and  $P=0$ . Therefore, the free-energy change for a pure element due to the switch is given by  $\Delta f_1$ , as in the second line of Eq. (2). The second step is also double: a reversible expansion of the repulsive gas, now at  $V_0$  and high pressure, to reach the dilute limit (where it becomes identical to the ideal gas), followed by a reversible compression of the ideal gas, to recover the initial density or volume. The change in free energy due to both processes is

$$\Delta f_2 = k_B T_0 \int_0^{\rho_0} \left[ \frac{P}{\rho k_B T_0} - 1 \right] \frac{d\rho}{\rho}, \quad (4)$$

where  $\rho_0 = N/V_0$  is the particle density. After the process represented by Eq. (4) has taken place we end up with an ideal gas at  $(T_0, \rho_0)$ , whose free energy  $f_{id}$  is known,

$$f_w^{\text{liq}}(T_0, \rho_0) = f_{id}(T_0, \rho_0) = k_B T_0 [\ln(\rho_0 \Lambda^3) - 1]. \quad (5)$$

Here  $\Lambda$  is the de Broglie thermal wavelength ( $\Lambda^2 = h^2/2\pi m k_B T_0$ ), where  $h$  is the Planck constant and  $m$  is the atomic mass.<sup>49</sup> Then the free energy of the liquid phase is calculated as the sum

$$g_L(T_0) = \Delta f_1 + \Delta f_2 + f_w^{\text{liq}}(T_0, \rho_0). \quad (6)$$

Equation (1), with Eqs. (2) and (6), give the free energies of the solid and liquid phases of pure elements as a function of temperature; with them, the melting points can be determined.

## ALLOYS

In this work we are interested on the Au-Ni solutions, a system with positive heat of mixing that may form either homogeneous or heterogeneous solutions in both solid and liquid phases. Therefore the lines of interest in the phase diagram are the liquids, the solidus, and the solvus (eventually in both phases). The strategy for the alloy calculations is to construct a set of free energy functions versus temperature  $g_c(T)$ , Eq. (1), for several values of the concentration  $c$ , extract from them  $g_T(c)$  curves for both phases, and then look at the common tangent construction.

In principle, Eq. (1) is readily applicable to alloys provided the sample is large enough to self-average the diversity of short-range configurations that appears in a real macroscopic sample. This is never the case for finite systems and therefore an important issue is to assess the dispersion in the final data originated by the choice of different initial samples. We come back to this point in the paragraph describing the simulations; at this moment let's assume that the sample is large enough to be representative of the thermodynamic limit and therefore the integral in the second term of the right-hand side (RHS) of Eq. (1) can easily be calculated. Similarly, the free energies of the reference systems (mixtures of Einstein oscillators or ideal gases) can be calculated using the following expression:<sup>48</sup>

$$f_{\text{Eins}}(c, T_0) = c f_{\text{Eins}}^{\text{Ni}} + (1-c) f_{\text{Eins}}^{\text{Au}} - T_0 s_{\text{conf}}(c). \quad (7)$$

for the Einstein crystal, where  $c$  measures the solute content (in what follows Ni is the solute), and  $f_{\text{Eins}}^{\text{Ni}}$  and  $f_{\text{Eins}}^{\text{Au}}$  are given by Eq. (3). The configurational entropy per particle  $s_{\text{conf}}(c)$ , is given by the usual expression  $k_B [c \ln(c) + (1-c) \ln(1-c)]$ , assuming the solution is completely random, i.e., no SRO appears; we come back to this point in the discussion session. For the ideal gas

$$f_{id}(c, T_0, \rho) = c f_{id}^{\text{Ni}}(\rho_{\text{Ni}}) + (1-c) f_{id}^{\text{Au}}(\rho_{\text{Au}}) \quad (8)$$

or, making the entropy of mixing appear explicitly,

$$f_{id}(c, T_0, \rho) = c f_{id}^{\text{Ni}}(\rho) + (1-c) f_{id}^{\text{Au}}(\rho) - T_0 s_{\text{conf}}(c), \quad (9)$$

where  $\rho$  is the total density,  $\rho_{\text{Ni}}$  and  $\rho_{\text{Au}}$  are the partial densities,  $c\rho$  and  $(1-c)\rho$ , respectively, and the  $f_{id}$ 's are given by Eq. (5). Note the different arguments of the  $f_{id}$ 's functions in Eqs. (8) and (9).

## REGULAR APPROXIMATION

In the regular approximation, the free energy per particle of a Au-Ni alloy with concentration  $c$  of Ni is given by

$$g_{\text{Reg}} = c g_{\text{Ni}}(T) + (1-c) g_{\text{Au}}(T) + \Delta h_{\text{xs}}(c, T) - T s_{\text{conf}}, \quad (10)$$

where  $g_{\text{Au}}(T)$  and  $g_{\text{Ni}}(T)$  are the free energy per particle of the pure elements. The first two terms in the RHS of Eq. (10) represent a linear interpolation between the pure constituents, i.e., the free energy of an ideal solution, and the last two terms are the excess free energy in the regular approximation, that measures the departure of the regular approximation from ideal behavior

$$\Delta g_{\text{Reg}}(c, T) = \Delta h_{\text{xs}}(c, T) - T s_{\text{conf}}. \quad (11)$$

Here the excess enthalpy of mixing per particle  $\Delta h_{\text{xs}}$  is the difference between the enthalpy of the actual mixture and the linear interpolation between the enthalpies of the pure elements, i.e., the enthalpy of the ideal solution

$$\Delta h_{\text{xs}}(c, T) = h_{\text{mix}}(c, T) - h_{id}(c, T),$$

$$h_{id}(c, T) = c h_{\text{Ni}} + (1-c) h_{\text{Au}}. \quad (12)$$

By definition, the difference between the free energy obtained in the exact calculation [Eq. (1) for the alloy] and that of the regular approximation [Eq. (10)] is equal to  $-T\Delta s_{\text{vib}}$ , where  $\Delta s_{\text{vib}}$  is the excess vibrational entropy, provided that the solution is random.

## SIMULATIONS

We use the EAM potentials of Foiles *et al.*<sup>45</sup> for our simulations. All samples have 256 atoms and the configurations for different values of the Ni concentration are obtained by Monte Carlo runs in the transmutation ensemble  $(T, P, N, \Delta\mu)$ , with  $N$  the total number of atoms and  $\Delta\mu$  the difference in chemical potential, adjusted to get the desired composition. Sufficiently long runs (longer than  $10^4$  MC steps/atom) allow the development of any eventual short-range order. Determinations of the Warren-Cowley SRO parameters during MC runs in the solid and liquid close to the phase transition indicate a null value for the nearest neighbor shell within the precision accessible with this sample size, in agreement with experimental findings.<sup>16</sup> The precision needed in free energy determinations, of the order of few meV/atom, crucially depends on the size of the sample. For different initial configurations of the finite sample, different values of the internal energy are obtained; fluctuations of these values at the sample size chosen are one of the main sources of error in the present work. To avoid this limitation larger samples, or averages over different samples as done in Ref. 40, are needed.

The temperature control in MD runs is provided by a thermostat based on a damping term whose strength and sign is determined by the difference between the actual and desired kinetic energies of the total sample. The center of mass motion, if any, is implicitly preserved by the equations of the motion for every step, so the initial condition has to be prepared with zero c.m. velocity. For long runs, this constraint is checked along the run and eventual departures are corrected. If the zero center of mass motion constraint is taken into account explicitly in the thermostat, then Eqs. (3) and (5) are no longer valid, and they have to be replaced by more involved expressions given in Ref. 50.

A constant-pressure simulation using the Parrinello-Rahman algorithm<sup>51</sup> and a time step of 2 fs is used in the simulations. In every run, the first  $10^4$  time steps are used to equilibrate the sample and the statistical average of the thermodynamic variables is obtained on an additional set of  $10^4$  time steps. In the case of the solid, the sample is heated in successive runs between 296 and 1800 K, with a temperature interval of 50 K. In every run, the enthalpy per particle for the solid  $h_s(T)$  is obtained. The same is done to determine the liquid phase internal enthalpy  $h_l(T)$ . In this case, the samples are heated up to 5000 K to melt them, and then cooled down from 2300 to 1600 K, in temperature steps of 50 K.

Second-order polynomials are adjusted to the simulation results of the internal enthalpy for solid and liquid Au-Ni alloys, see Fig. 1, and the integral of Eq. (1) is solved analytically. The resulting Gibbs free energies per particle are computed as

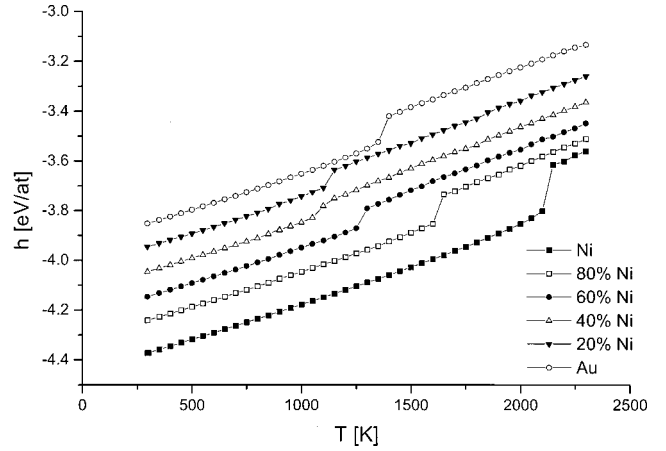


FIG. 1. Temperature dependence of the enthalpy per particle of solid and liquid different Au-Ni alloys (heating runs).

$$g(T) = g(T_0)(T/T_0) - T[a_2(T - T_0) + a_1 \ln(T/T_0) - a_0(1/T - 1/T_0)], \quad (13)$$

where  $a_i$  are the polynomial coefficients of a quadratic fit to the enthalpies reported in Fig. 1. They are given in Table I, together with the quantities entering  $g(T_0)$  in Eq. (13).

The reference free energy of the solids  $g(T_0)$  is calculated at  $T_0 = 296$  K using Einstein temperatures  $T_E^{\text{Ni}} = 200$  K and  $T_E^{\text{Au}} = 100$  K. The Einstein temperature is chosen to minimize the structure of the switch curve in order to improve the numerical precision, which in this scale has to be a few meV atom. Sturgeon and Laird<sup>4</sup> propose a systematic way to choose the Einstein temperature: the best value is that giving a mean-squared displacement similar to the value obtained with the EAM interactions.

To calculate the switch, we first cool down the samples to 0 K at the volume corresponding to  $P = 0$  at  $T = 296$  K and determine the equilibrium positions  $\{r_{i0}\}$  of the Einstein crystal. Typically, we calculate the average  $\langle U - W_{\text{so}} \rangle$  at constant temperature and constant volume, for values of  $\lambda$  varying between 0 and 1 with an interval  $\Delta\lambda = 0.05$ . Again, the calculations at a given  $\lambda$  are carried out in two successive runs each of  $10^4$  steps and averages  $\langle U - W_{\text{so}} \rangle$  are taken on the second set of time steps. We fit a polynomial curve of fifth degree to these points and solve the integral of Eq. (2) analytically.

In the liquid phase, the Helmholtz free-energy change  $\Delta f_1$  is evaluated at a reference temperature  $T_0 = 2300$  K. The average volume,  $V_{\text{av}}$  of a sample equilibrated at 2300 K is used to generate a cubic sample with volume  $V_0 = V_{\text{av}}(2300 \text{ K})$ . This cubic sample is taken as the starting sample for each run for every value of  $\lambda$ . The switching parameter  $\lambda$  varies between 0 and 1, in intervals of 0.05, and before each  $\langle U - W_{\text{liq}} \rangle$  average process we equilibrate the sample, as for the solid case. A sixth degree polynomial is fitted to the points and the integral of Eq. (2) is solved analytically. We then expand the sample keeping the temperature constant and equal to  $T_0$ . This is done in 14 consecutive runs reducing the pressure from about 125 to 2 kbar. At every step two successive runs of  $10^4$  time steps each are carried out.

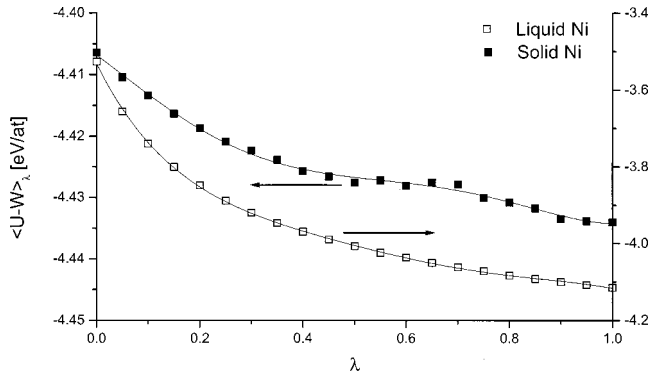


FIG. 2. Example of the integrand  $\langle U-W \rangle_\lambda$  appearing in the switching Hamiltonian method, Eq. (2), versus the switching parameter  $\lambda$ , corresponding to the liquid (right axis) and solid (left axis) phases of pure Ni.

The average pressure, density, and temperature are obtained during the second run. Two more values are added to this data: the origin ( $P=0, \rho=0$ ), corresponding to the ideal gas limit, and the average pressure and density obtained for the case  $\lambda=0$ . Once the evolution of pressure as a function of density is obtained, we proceed to calculate the integrand of Eq. (4)  $P/\rho k_B T - 1$ , and to fit a sixth degree polynomial to this function. The Helmholtz free-energy change  $\Delta f_2$  is obtained by the analytical integration of this polynomial.

## RESULTS

The MD simulations carried out for several Au-Ni alloy compositions show a smooth behavior of the solid and liquid internal enthalpies  $h_S$  and  $h_L$  as a function of temperature when the concentration changes, see Fig. 1. A step shows the temperature at which the solid becomes a liquid. These steps do not reflect the thermodynamic melting but the melting temperature for those particular conditions of the simulation. The points shown in the figure correspond to heating runs, from room temperature up to 2300 K. These points are the integrand appearing in Eq. (1). On cooling, the points overlap, except by a hysteresis in the solid-liquid transitions related to the overheating-undercooling phenomena. The latent heat of melting for pure Ni is 0.191 and 0.101 eV/at. for Au in good agreement with the experimental values of 0.182 and 0.128 eV/at. found in the literature.<sup>14</sup>

The integrand for the switching Hamiltonians, Eq. (2), is shown in Fig. 2 for pure Ni in the solid phase. The shape of these curves satisfy the Bogoliubov inequality  $\langle \partial^2 H(\lambda) / \partial \lambda^2 \rangle < 0$ ,<sup>48</sup> which is used to test the accuracy of the integrand. For the solid phase, the region  $\lambda \sim 1$  is difficult to get with a good precision because the average Hamiltonian determining the equations of motion in this case is close to  $U$  (the EAM), while one of the magnitudes to be averaged is  $W$ , the term coming from the Einstein oscillators.  $U$  is independent of the center of mass motion, but  $W$  is very sensitive to it, so the  $\lambda \sim 1$  limit, and then the integral, has significant errors. Similarly, in the liquid phase, the switch to the repulsive gas depends on the strength of the repulsive potential, which is adjusted to avoid crystallization and atom overlap,

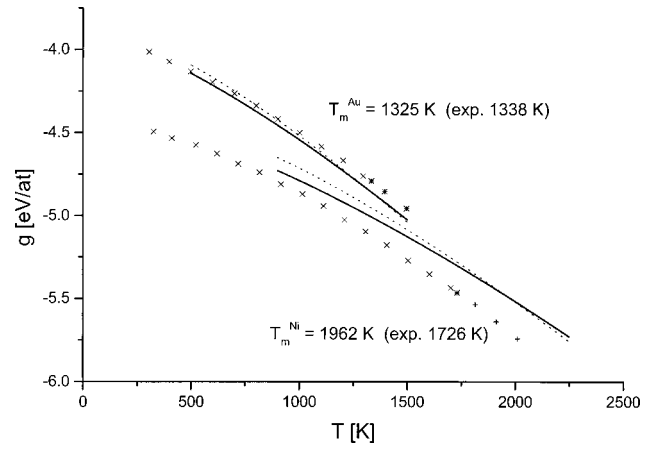


FIG. 3. Calculated and experimental (Ref. 16) Gibbs free energy per particle  $g_S$  and  $g_L$  for solid and liquid phases of pure Ni and Au.

and at the same time to minimize the structure of the integrand in Eq. (2). The role of the thermostat in this procedure is crucial; the Einstein oscillators do not thermally equilibrate among themselves because they are independent, only the  $\lambda U$  part of the Hamiltonian leads to equipartition. Therefore the precision of the integral becomes a difficult issue for small  $\lambda$  and long equilibration runs are needed. The Langevin thermostat is a good option to avoid this difficulty.

The free-energy functions  $g_S(T)$  and  $g_L(T)$  for the solid and liquid phases of the pure elements are shown in Fig. 3. The melting temperature  $T_m$  is obtained from the intersection of these curves. Au free energies cross at  $T_m^{Au} = 1325$  K, 13 K (1%) below the experimental melting point  $T_m^{exp} = 1337.6$  K. The intersection of Ni free energies gives  $T_m^{Ni} = 1962$  K, which is 236 K (14%) bigger than the experimental melting point  $T_m^{exp} = 1726$  K.

The calculated values of the excess enthalpy of mixing per particle  $\Delta h_{xs}$ , Eq. (12), are shown in Fig. 4 as a function of the Ni concentration. We obtain  $\Delta h_{xs}$  positive and smaller than the experimental value for the solid, and negative—

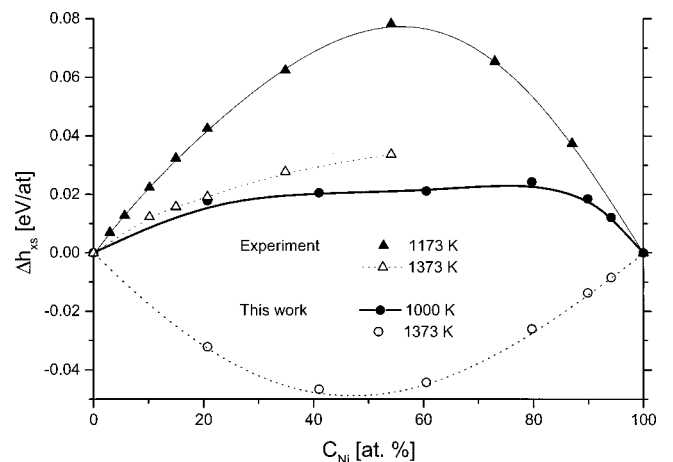


FIG. 4. Calculated (circles) and experimental (triangles) (Ref. 16) excess enthalpy of mixing for solid and liquid Au-Ni alloys. Filled and empty marks correspond to the solid and liquid phases, respectively.

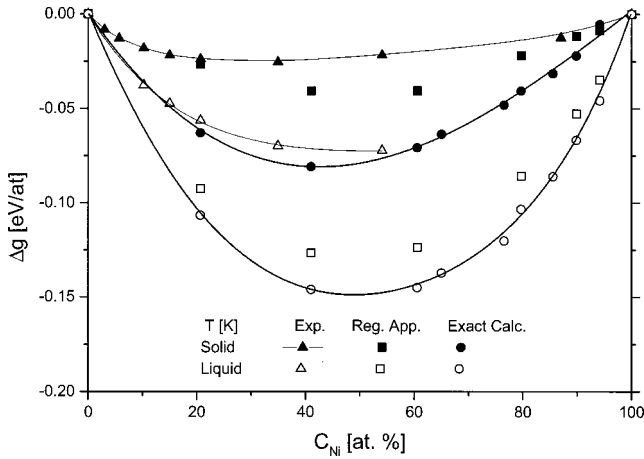


FIG. 5. Excess free energy  $\Delta g$  of solid and liquid Au-Ni alloys at two different temperatures: (circles) exact calculation, (squares) regular approximation, (triangles) experimental results taken from Ref. 16.

contrary to experiments—for the liquid. Positive values of  $\Delta h^{xs}$  for the solid indicate a tendency for phase separation, and the possible existence of a miscibility gap. We report the excess enthalpy for the solid phase at  $T=1000$  K since at higher temperatures the alloys with low concentration of Ni are already liquid. The figure shows a maximum at  $c \approx 0.8$  for the solid, a more pronounced asymmetry than the experimental one. Excess enthalpies of both solid and liquid phases, obtained from our MD simulations for these potentials, are smaller than the experimental values reported by Bienzle *et al.*<sup>16</sup> In particular, MD simulations show that unlike atoms attract each other in the liquid leading to negative values of  $\Delta h_{xs}$ . This tendency increases as temperature increases.

Small values of excess enthalpy for solid and liquid solutions lead to smaller (more negative) values of excess free energy  $\Delta g(c, T)$ , either in the regular approximation, Eq. (11), or in the exact calculation. This is shown in Fig. 5, where we compare both calculations with the experimental results for solid ( $T=1073$  K) and liquid ( $T=1373$  K) phases.<sup>16</sup>

Figure 5 also shows that the results in the regular approximation (squares) are closer to the experiment (up triangles) than the values obtained with the exact calculation for both solid and liquid phases. The difference between the exact results and regular approximation indicates a significant influence of the vibrational entropy. From the difference in free energy between the regular approximation and the exact calculation, we determine the vibrational entropy; see Fig. 6. The results of MD simulations and the experimental values<sup>16</sup> for both solid and liquid Au-Ni alloys show remarkable agreement.

The relative magnitudes of the excess free energy in the liquid and in the solid, determine the nature of the phase diagram. We present first the results in the regular approximation. The predictions for the Au-Ni phase diagram are shown in Fig. 7, together with the experimental results from Ref. 16. The diagram exhibits a two-phase solid-liquid region with a minimum at the congruent point located at  $c$

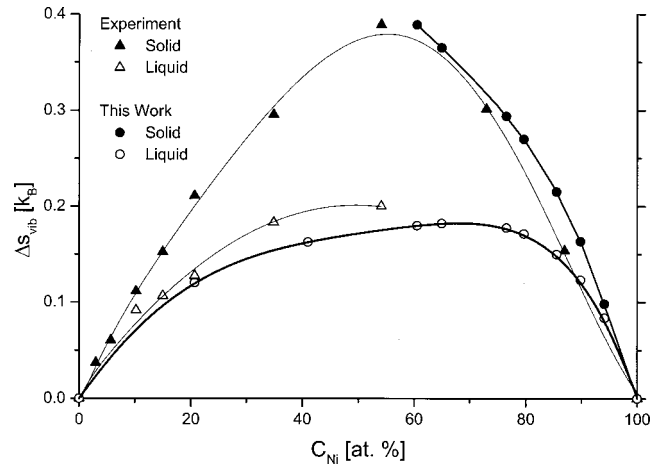


FIG. 6. Calculated and experimental entropy of solid ( $T=1173$  K) and liquid ( $T=1373$  K) Au-Ni alloys.

$\sim 0.41$ , in excellent agreement with the experimental value  $c=0.425$ , and at  $T \sim 850$  K, well below the experimental value  $T=1228.15$  K. The enhanced stability of the liquid (negative excess enthalpy) is at the origin of this discrepancy; in fact  $\Delta g_L$  is much more negative than the experimental value and intersects the solid free energy at a much lower temperature. The splitting between solidus and liquidus is also more pronounced. The much higher melting point of Ni is an additional major difference.

In the solid region a miscibility gap appears. Always in the regular approximation, the gap extends to temperatures very close to the *solidus*. We have a *solvus* curve with a critical temperature  $T_c \sim 900$  K at  $c \sim 0.73$ . The experimental value is  $T_c = 1083.45$  K at  $c = 0.706$ . Also, the experimental miscibility gap extends over a larger range of low Ni concentrations than that found in this regular approximation. The precision of these determinations is such that it could also have predicted a contact between the *solvus* and the *solidus*, giving a peritectic system with an invariant horizontal line in the phase diagram located at  $T \sim 900$  K. This is due to the fact that the congruent point is 400 K lower than the experiment for the reasons mentioned above.

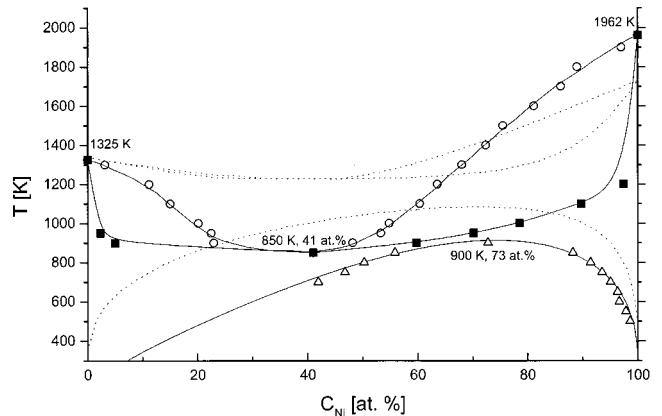


FIG. 7. Au-Ni phase diagram in the regular approximation—*solidus-liquidus* and *solvus* curves. The experimental phase diagram (broken lines) (Ref. 16) is shown for comparison.

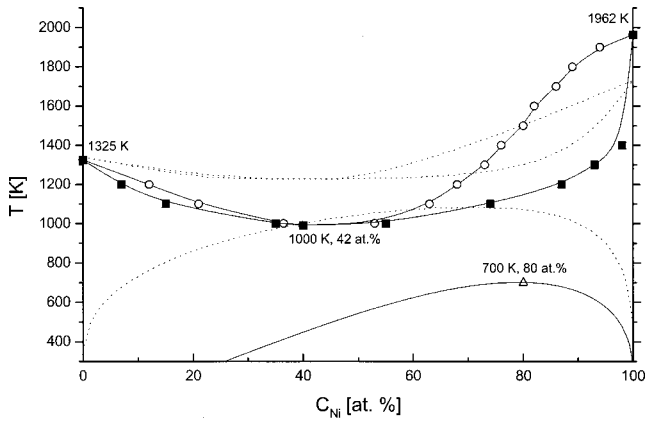


FIG. 8. Au-Ni phase diagram in the exact calculation. The experimental phase diagram (broken lines) (Ref. 16) is shown for comparison.

Finally, we compare the results obtained in the exact calculation with the experimental phase diagram, see Fig. 8. Considering the large positive excess entropy contribution, it is to be expected that the exact result differ significantly from the regular approximation. The exact calculation shows that the region of two phases is very narrow in the region of low Ni concentration. The congruent point is found at the same concentration,  $c \sim 0.42$ , but at higher temperature,  $T \sim 1000$  K, than in the regular approximation, which is consistent with the larger excess entropy for the solid than for the liquid (see Figure 6) that corrects in part the negative mixing enthalpy of the liquid. The *solvus* has a critical temperature of  $\sim 700$  K at approximately the same composition,  $c \sim 0.8$ , as in the regular approximation. In both calculations, the location on the  $c$  axis of the congruent and critical points is in fairly good agreement with the experiments.

## DISCUSSION

We presented the exact phase diagram of a model Hamiltonian. Two different aspects have to be discussed now. The first aspect is related to the precision of the method to reveal the true phase diagram of the model, a question that arises naturally considering the sensitivity of these results to small errors in the calculated values (a few meV/atom in free energies translates into 50–100 K in the location of the points in the phase diagram). The second aspect concerns the ability of the model to reproduce the features of the real system.

The precision of the phase diagram is even more relevant considering that for the same potentials, Foiles and Adams reported for Ni a melting point of 1740 K,<sup>45</sup> while we find 1962 K, and for Au they report 1090 K while our value is 1325 K. There are several simpler ways to calculate melting points with precision, which can be used to check the validity of the complex way used in this work. In particular, a Monte Carlo simulation with the EAM potential and full relaxation shows the transition temperature through the crystalline order parameter (a parameter that projects the position of the atoms in a subspace corresponding to a fcc lattice regardless of their chemical nature). This procedure can be applied to both pure elements and to the alloy at the congru-

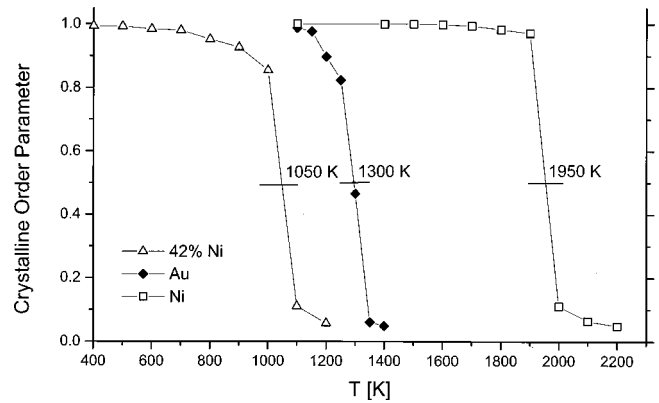


FIG. 9. Monte Carlo calculations of crystalline order parameter showing the melting temperatures of the pure elements and the alloy at 42% Ni content, the congruent melting point.

ent composition. These results are shown in Fig. 9 indicating a remarkable agreement between these three values and those extracted from the phase diagram, Figs. 7 and 8. This constitutes a robust validation of our results.

Although these three points of the phase diagram are quite precise, the location of almost every other point, especially on the *solidus* line is affected by significant errors. The main source of them is the sample size, that induces fluctuations in the trend curve of enthalpy versus composition, Fig. 4, of a few meV/atom depending on which sample is taken from the Monte Carlo generation process. These fluctuations disappear in the thermodynamic limit by self-averaging of local order arrangements, but for a sample with 256 atoms, they are important. A way to overcome this limitation is to repeat the procedure for several samples, and then take average values, as done in Ref. 40; other way is to increase the size of the sample. Another source of error in the location of the *solidus* line is the fact that we calculated a small set of concentrations, namely, 0, 20, 40, 60, 80, 90, 95, and 100% Ni, while for a proper determination of the *solidus*, more values of  $c$  would have been needed to account for the sensitive behavior of  $g$  originated in the infinite derivative of the entropy of mixing close to  $c=0$  and  $c=1$ . Analytic error determination associated to the phase diagrams, Figs. 7 and 8, is not possible because the location of phase boundaries is the result of a geometric construction (the common tangent construction). However, qualitative error estimation is suggested through the size of the symbols used in these figures, representing approximately  $25^\circ$  in temperature and 2% in concentration. Similarly, the data in figs. 2, 4–6, are affected by 2–3 meV/atom error, as suggested by the symbol size.

In Fig. 6 we obtained the vibrational contribution to the entropy as the difference between the exact result and the regular approximation in excellent agreement with the experiments. Alternatively, the derivative of the free energy  $g(T, c)$  with respect to temperature equals minus the entropy.  $S = S_{\text{conf}} + S_{\text{vib}}$  can then be calculated for all concentrations and temperatures using the data of Table I. Following this way we get essentially the same values for  $S_{\text{vib}}$  reflecting the consistency of the data.

Additionally, the entropy difference between the two phases of the pure elements at the melting point times  $T_m$  is

TABLE I. Free-energy parameters at the reference temperature  $T_0$ . Energy changes of the Hamiltonian switch ( $\Delta f_1$ ) and reversible expansion ( $\Delta f_2$ ). Einstein crystal ( $f_{\text{Eins}}$ ) and ideal gas ( $f_{\text{id}}$ ) free energies. Coefficients  $a_i$  of the free-energy calculations.

$T_0 = 296 \text{ K}$	$g_S(T_0)$	$\Delta f_1$	$f_{\text{Eins}}$	$a_2$	$a_1$	$a_0$	
0% Ni	-4.01488	-3.93184	-0.08304	$4.13928 \times 10^{-8}$	$2.30470 \times 10^{-4}$	-3.92296	
20% Ni	-4.11310	-4.02803	-0.08507	7.08464	1.94317	-4.00833	
40% Ni	-4.20338	-4.12483	-0.07855	5.24308	2.11667	-4.11171	
60% Ni	-4.28534	-4.21730	-0.06804	3.16491	2.37220	-4.21880	
75% Ni	-4.34837	-4.29205	-0.05632	2.62324	2.44480	-4.30145	
80% Ni	-4.35838	-4.30473	-0.05365	3.38929	2.29682	-4.31105	
85% Ni	-4.38367	-4.33547	-0.04820	2.45152	2.43717	-4.34937	
90% Ni	-4.40169	-4.35792	-0.04377	2.76865	2.38583	-4.37273	
95% Ni	-4.42410	-4.38530	-0.03880	2.50231	2.41022	-4.40193	
100% Ni	-4.45485	-4.42485	-0.03000	2.50614	2.40940	-4.44497	
$T_0 = 2300 \text{ K}$	$g_L(T_0)$	$\Delta f_1$	$\Delta f_2$	$f_{\text{id}}$	$a_2$	$a_1$	$a_0$
0% Ni	-5.97886	-3.67856	0.66609	-2.96639	$-2.16607 \times 10^{-8}$	$3.98586 \times 10^{-4}$	-3.93358
20% Ni	-6.09640	-3.77319	0.65557	-2.97878	-2.19563	3.99809	-4.06636
40% Ni	-6.11691	-3.84434	0.65168	-2.92425	-2.33022	4.11734	-4.19213
60% Ni	-6.08372	-3.89789	0.65164	-2.83747	-2.39753	4.23915	-4.29897
75% Ni	-6.01545	-3.93360	0.65930	-2.74115	1.77105	2.79347	-4.24693
80% Ni	-5.99472	-3.93596	0.66101	-2.71977	-2.00220	4.24640	-4.38253
85% Ni	-5.95677	-3.94614	0.66465	-2.67528	-1.41262	4.11276	-4.40098
90% Ni	-5.92507	-3.95569	0.66941	-2.63878	-1.55162	4.19990	-4.42130
95% Ni	-5.88758	-3.95994	0.67089	-2.59853	-0.83478	3.98417	-4.41992
100% Ni	-5.80695	-3.96158	0.68269	-2.52806	-2.20455	4.54990	-4.49225

the latent heat of melting. From Eq. (13) for  $g(T)$ , the coefficients  $a_i$  from Table I, and  $T_m$  from Fig. 3, we get the latent heat of melting  $L$  for Au,  $L_{\text{Au}} = 0.101 \text{ eV/at.}$ , and for Ni  $L_{\text{Ni}} = 0.191 \text{ eV/at.}$ , in good agreement with the experimental values  $0.128 \text{ eV/at.}$  for Au and  $0.183 \text{ eV/at.}$  for Ni.

It is curious then that while this alloy is poorly described in terms of the enthalpy of mixing of both liquid and solid phases, the entropy is in excellent agreement with the experiments. In fact, Fig. 4 shows that in the enthalpy of solid phase there is approximately a factor 3 to 4 between prediction and experiment, despite the fact that the dilute heats of solution (i.e., the derivatives of this curve at  $c=0$  and  $c=1$ ) are correct because they were used as input data in the fitting procedure of the potentials. But the prediction is much worse for the liquid phase, where these EAM potentials predict a negative excess enthalpy of mixing, against a positive—although much smaller than in the solid phase—value found experimentally. This curiosity is probably related to the facts described in the introduction in the sense that Au-Ni has a cancellation of two large contributions to the enthalpy of mixing, namely, the size effect and the chemical effect. Somehow, the EAM is capturing an aspect of reality that is able to describe the vibrations of the alloy (that is the derivatives of the energy) but is unable to describe the energetics itself.

Not only are the vibrations well described, but the order is too. The nearest-neighbor Warren-Cowley SRO parameter close to (but below) the congruent melting temperature gives a value close to zero and negative ( $-0.044$ ); this reflects a

small tendency to ordering in an alloy which is phase separating at lower temperatures. *Ab initio* calculations by Wolverton *et al.*<sup>28</sup> gave values similar to these. The experiment is also close to zero but positive. For the second shell, the experiment gives a positive value,  $0.148$ , while the *ab initio* result is  $0.120$ . This EAM potential gives a positive value but smaller than the experiment:  $0.05$ . It is curious that the *ab initio* and EAM show a change in sign between the SRO parameter of the first and second shell, ordering and clustering tendency respectively, while the experimental values are both positive. For the liquid, the fact that the excess enthalpy is negative may give a SRO showing tendency to ordering. This is what happens at  $1023 \text{ K}$  and  $c \sim 0.4$ , the SRO is  $-0.033$ , a small tendency to ordering.

In summary we presented an exact calculation of the phase diagram of a model Hamiltonian, namely, the EAM potential for Au-Ni of Foiles *et al.*<sup>45</sup> We find an overall qualitative agreement in the characteristics of the phase diagram: a *solidus-liquidus* with a large splitting and with a deep minimum at the right concentration, a *solvus* with the right concentration at the critical temperature, and reasonable values for the melting temperatures of the pure constituents. However, the wrong enhanced stability of the liquid with respect to the ideal mixture, drops the position of the liquid free energy, intersecting the solid one at lower temperatures; consequently the location on the temperature axis of the characteristic points of the phase diagram is approximately  $300 \text{ K}$  below the experimental values.

## ACKNOWLEDGMENTS

We acknowledge fruitful discussions with P. Turchi and R. Passianot. The hospitality at the Atomistic Simulation Group, Queen's University Belfast, where part of this work was done, is gratefully acknowledged. One of us (E.O.)

acknowledges the hospitality at Centro Atómico Bariloche, the Agencia Española de Cooperación Internacional, and the Spanish Ministerio de Educación y Cultura (Grant No. PB98-0780-c02) for financial support. One of us (A.C.) acknowledges financial support from the Leverhulme Trust. This work was partially supported by CONICET, Grants No. PIP 4205/96 and PIP 0664/98.

- <sup>1</sup>M. S. Daw and M. I. Baskes, *Phys. Rev. B* **29**, 6443 (1984).
- <sup>2</sup>M. W. Finnis and J. E. Sinclair, *Philos. Mag. A* **50**, 45 (1984).
- <sup>3</sup>F. Ercolessi, M. Parrinello, and E. Tosatti, *Philos. Mag. A* **58**, 213 (1988).
- <sup>4</sup>J. B. Sturgeon and B. B. Laird, *Phys. Rev. B* **62**, 14 720 (2000).
- <sup>5</sup>D. Farkas, B. Mutasa, C. Vailhe, and K. Ternes, *Modell. Simul. Mater. Sci. Eng.* **3**, 201 (1995).
- <sup>6</sup>R. S. Averback and T. Díaz de la Rubia, in *Solid State Physics*, edited by H. Ehrenreich and F. Spaepen (Academic, New York, 1998), Vol. **51**, p. 281.
- <sup>7</sup>E. E. Zhurkin and M. Hou, *J. Phys.: Condens. Matter* **12**, 6735 (2000).
- <sup>8</sup>J. M. Campillo, S. Ramos de Debiaggi, and A. Caro, *J. Mater. Res.* **14**, 2849 (1999).
- <sup>9</sup>M. Asta and S. M. Foiles, *Phys. Rev. B* **53**, 2389 (1996).
- <sup>10</sup>C. Wolverton and A. Zunger, *Comput. Mater. Sci.* **8**, 107 (1997).
- <sup>11</sup>P. A. Flinn, B. L. Averbach, and M. Cohen, *Acta Metall.* **1**, 664 (1953).
- <sup>12</sup>R. A. Oriani and W. K. Murphy, *J. Phys. Chem.* **62**, 199 (1958).
- <sup>13</sup>A. Münster and K. Sagel, *Z. Phys. Chem. (Leipzig)* **14**, 296 (1958).
- <sup>14</sup>R. Hultgren, R. L. Orr, P. D. Anderson, and K. K. Kelly, in *Selected Values of Thermodynamic Properties of Metals and Alloys* (Wiley, New York, 1963), p. 476.
- <sup>15</sup>H. Okamoto and T. B. Massalski, in *Phase Diagrams of Binary Gold Alloys* (ASM International, Metals Park, OH, 1987), p. 193.
- <sup>16</sup>M. Bienzle, T. Oishi, and F. Sommer, *J. Alloys Compd.* **220**, 182 (1995).
- <sup>17</sup>W. Köster and W. Dannöhl, *Z. Metallkd.* **9**, 248 (1936).
- <sup>18</sup>F. Hofer and P. Warbichler, *Z. Metallkd.* **76**, 11 (1985).
- <sup>19</sup>N. B. Chanh and J. P. Bastide, *Bull. Soc. Chim. Fr.* **5**, 1911 (1968).
- <sup>20</sup>T. B. Wu, J. B. Cohen, and W. Yelon, *Acta Metall.* **30**, 2065 (1982).
- <sup>21</sup>T. B. Wu and J. B. Cohen, *Acta Metall.* **32**, 861 (1984).
- <sup>22</sup>V. V. Sanadze and G. V. Gulyaev, *Sov. Phys. Crystallogr.* **4**, 496 (1960).
- <sup>23</sup>S. Takizawa, K. Terakura, and T. Mohri, *Phys. Rev. B* **39**, 5792 (1989).
- <sup>24</sup>Z. W. Lu and A. Zunger, *Phys. Rev. B* **50**, 6626 (1994).
- <sup>25</sup>G. Abadias, I. Schuster, A. Marty, and B. Gilles, *Phys. Rev. B* **61**, 6495 (2000).
- <sup>26</sup>C. Amador and G. Bozzolo, *Phys. Rev. B* **49**, 956 (1994).
- <sup>27</sup>C. Colinet, J. Eymery, A. Pasturel, A. T. Paxton, and M. van Schilfgaarde, *J. Phys.: Condens. Matter* **6**, 47 (1994).
- <sup>28</sup>C. Colinet, A. Pasturel, *J. Alloys Compd.* **296**, 6 (2000).
- <sup>29</sup>C. Wolverton, V. Ozolins, and A. Zunger, *Phys. Rev. B* **57**, 4332 (1998).
- <sup>30</sup>T. B. Wu and J. B. Cohen, *Acta Metall.* **32**, 861 (1984).
- <sup>31</sup>D. Frenkel and A. J. C. Ladd, *J. Chem. Phys.* **81**, 3188 (1984).
- <sup>32</sup>W. G. T. Kranendonk and D. Frenkel, *J. Phys.: Condens. Matter* **1**, 7735 (1989).
- <sup>33</sup>J. Mei, J. W. Davenport, *Phys. Rev. B* **46**, 21 (1992).
- <sup>34</sup>R. M. Lynden-Bell, J. S. van Duijneveldt, and D. Frenkel, *Mol. Phys.* **80**, 801 (1993).
- <sup>35</sup>M. de Koning and A. Antonelli, *Phys. Rev. E* **53**, 465 (1996).
- <sup>36</sup>M. de Koning and A. Antonelli, *Phys. Rev. B* **55**, 735 (1997).
- <sup>37</sup>M. de Koning, A. Antonelli, and S. Yip, *Phys. Rev. Lett.* **83**, 3973 (1999).
- <sup>38</sup>A. D. Bruce, N. B. Wilding, and G. J. Ackland, *Phys. Rev. Lett.* **79**, 3002 (1997).
- <sup>39</sup>G. D. Barrera and R. H. de Tandler, *Comput. Phys. Commun.* **105**, 159 (1997).
- <sup>40</sup>G. D. Barrera, R. H. de Tandler, and E. P. Isoardi, *Modell. Simul. Mater. Sci. Eng.* **8**, 389 (2000).
- <sup>41</sup>N. L. Allan, G. D. Barrera, R. M. Fracchia, M. Yu. Lavrentiev, M. B. Taylor, I. T. Todorov, and J. A. Purton, *Phys. Rev. B* **63**, 094203 (2001).
- <sup>42</sup>N. L. Allan, G. D. Barrera, M. Yu. Lavrentiev, I. T. Todorov, and J. A. Purton, *J. Mater. Chem.* **11**, 63 (2001).
- <sup>43</sup>G. K. Straub, J. B. Aidun, J. M. Wills, C. R. Sanchez-Castro, and D. C. Wallace, *Phys. Rev. B* **50**, 5055 (1994).
- <sup>44</sup>G. A. De Wijs, G. Kresse, and M. J. Gillan, *Phys. Rev. B* **57**, 8223 (1998).
- <sup>45</sup>S. M. Foiles, M. I. Baskes, and M. S. Daw, *Phys. Rev. B* **33**, 7983 (1986).
- <sup>46</sup>S. M. Foiles and J. B. Adams, *Phys. Rev. B* **40**, 5909 (1989).
- <sup>47</sup>M. Asta and S. M. Foiles, *Phys. Rev. B* **53**, 2389 (1996).
- <sup>48</sup>*Molecular-Dynamics Simulation of Statistical-Mechanical Systems*, edited by G. Ciccotti and W. G. Hoover (North-Holland, Amsterdam, 1986), pp. 169–178.
- <sup>49</sup>D. Frenkel and B. Smit, *Understanding Molecular Simulation—From Algorithms to Applications* (Academic Press, London, 1996).
- <sup>50</sup>E. Ogando, M. Caro, and A. Caro (unpublished).
- <sup>51</sup>M. Parrinello and A. Rahman, *J. Appl. Phys.* **52**, 7182 (1981).